RSC Advances

PAPER

View Article Online
View Journal | View Issue

Cite this: *RSC Adv.*, 2022, **12**, 3136

Antimicrobial activity of silver sulfide quantum dots functionalized with highly conjugated Schiff bases in a one-step synthesis†

Nurulizzatul Ningsheh M. Shahri,[a] Hussein Taha,[b] Malai Haniti S. A. Hamid,[a] Eny Kusrini,[c] Jun-Wei Lim,[d] Jonathan Hobley[e] and Anwar Usman *[a]

In the present paper, low-dimensional Ag_2S QDs were fabricated for the first time, with four different dithiocarbazate derivative Schiff bases (SB) as capping agents in a one-pot synthesis. These SB-capped Ag_2S QDs were almost spherical with an average size range of 4.0 to 5.6 nm, which is slightly smaller than conventional thioglycolic acid (TGA)-capped Ag_2S QDs. We demonstrate that the growth of Gram-positive bacteria (*Bacillus subtillus* and *Staphylococcus aureus*), Gram-negative bacteria (*Escherichia coli* and *Pseudomonas aeruginosa*), and a prevalent fungal pathogen (*Candida albicans*) are inhibited more when the bacterial and fungal cells were nurtured with the synthesized SB-Ag_2S QDs, compared with TGA-Ag_2S QDs or free unbound Schiff bases. The minimum inhibitory concentration (MIC) results confirmed that even low concentrations of SB-Ag_2S QDs were able to inhibit bacterial (MIC 5–75 μg mL^{-1}) and fungal growth (MIC 80–310 μg mL^{-1}), and in some cases they performed better than streptomycin (8–25 μg mL^{-1}). Lethality bioassay results confirmed that SB-Ag_2S QDs were not toxic to brine shrimp (*Artemia salina*). The results show that capping agents are essential in the design of functional Ag_2S QDs, and highlight that Schiff bases provide an excellent opportunity to optimize the biological activities of silver based QDs.

Received 11th November 2021
Accepted 14th January 2022

DOI: 10.1039/d1ra08296e

rsc.li/rsc-advances

1. Introduction

In general, photo-excited quantum dots (QDs) emit bright, sharp and tunable light emission from the UV to the near infrared (NIR) making them suitable for bioimaging. In particular, they can be used to substitute toxic synthetic dyes in diagnostics, cancer therapies,[1] and as antibacterial agents.[2] Among them, silver sulfide (Ag_2S) QDs have received much attention for biomedical applications, due to their high chemical stability,[3] good photo-stability,[4] broad optical absorption spectrum,[5,6] and non-toxic properties.[7] With their narrow band-gap energy (~1 eV),[8] Ag_2S QDs are the most important nanometer-sized materials to be developed for biocompatible NIR-QDs for *in vivo* optical imaging.[9–13] In addition, under intense light excitation they produce a large photothermal effect and have good heat dissipation properties which makes them potential candidates for *in situ* photothermal cancer therapeutics.[2,14] The great promise of Ag_2S QDs in biomedical applications demands further explorative and challenging research, in order to realize their full potential.

It has been demonstrated that capping agents play an important role in developing photostable QDs.[15] However, capping agents can also be used to harness and control chemical reactions on their surface.[16] For example, CdS QDs capped with thiols, nitroxides, and surfactants can be used to detect peptides, tyrosine, cysteine, and organic radicals.[17,18] In addition, QDs capped with biodegradable, biocompatible, and compounds with low toxicity from bacteria[19] or plant leaves[20] have been used to supress the growth of A549 lung cancer cell.[20] In this vein, Schiff bases also offer an opportunity to be used as a strategic design of capping agents as they also exhibit antimicrobial,[21,22] antifungal,[23,24] anti-inflammatory,[25] and anticancer activities.[26] Furthermore, conjugated Schiff bases, with a corresponding reduction in their LUMO level may promote electron transfer from the Ag_2S core which may enhance the anti-pathogen activities of the QD. This is because the Fermi level of Ag_2S is high in energy (absolute level ~10 eV as determined by photoelectron spectroscopy) and the bandgap is low enough in energy that the conduction band is easily populated

[a]*Chemical Sciences, Faculty of Science, Universiti Brunei Darussalam, Jalan Tungku Link, Gadong BE1410, Brunei Darussalam. E-mail: anwar.usman@ubd.edu.bn*
[b]*Environmental and Life Sciences, Faculty of Science, Universiti Brunei Darussalam, Jalan Tungku Link, Gadong, BE1410, Brunei Darussalam*
[c]*Department of Chemical Engineering, Faculty of Engineering, Universitas Indonesia, Kampus Baru UI-Depok, 16424, Indonesia*
[d]*Department of Fundamental and Applied Sciences, HICoE-Centre for Biofuel and Biochemical Research, Institute of Self-Sustainable Building, Universiti Teknologi PETRONAS, 32610 Seri Iskandar, Perak Darul Ridzuan, Malaysia*
[e]*Department of Biomedical Engineering, National Cheng Kung University, 1, University Road, Tainan City 701, Taiwan, ROC*

† Electronic supplementary information (ESI) available. See DOI: 10.1039/d1ra08296e

at room temperature.[8,27,28] For this reason Ag_2S has often been used as an electron injector or shuttle in hybrid catalytic and light harvesting systems.[27,28]

Size-controlled Ag_2S QDs have been synthesized by various methods, including the single precursor,[3] one-pot synthesis,[29] hydrothermal,[30] water-phase microwave,[31] liquid–liquid interface reaction,[32] and reverse microemulsion methods.[33,34] The capping agents used to passivate the atoms on the QD surface, which are important to stabilize and prevent the nanocrystalline structures from aggregating, include surfactant (cetyltrimethyl ammonium bromide),[35] sodium dodecyl sulfate,[36] Schiff-base (2-(benzylidene amino)azobenzothiol) ligand,[37] ethylenediaminetetraacetic acid (EDTA),[38] 2-mercaptopropioic acid (2-MPA),[10,39] thioglycolic acid (TGA),[40] and or a carbon-containing shells.[41]

The objective of this study was to develop NIR active Ag_2S QDs in a one-pot synthesis with four different Schiff bases (SB) as stabilizing agents. These SB-Ag_2S QDs are reported for the first time. The SB-Ag_2S QDs were screened for antibacterial activity against Gram-positive and Gram-negative, namely *Bacillus subtilis*, *Pseudomonas aeruginosa*, *Escherichia coli*, and *Staphylococcus aureus* bacterial strains, as well as for their antifungal activities against *Candida albicans*. The detailed antimicrobial activities of the SB-Ag_2S QDs were further evaluated by determining their minimum inhibitory concentration (MIC) and minimum bactericidal concentration (MBC). The cytotoxicity of the SB-Ag_2S QDs was assessed using the brine shrimp lethality bioassay. The results were systematically evaluated and compared with the antimicrobial activities of the conventional TGA-capped Ag_2S QDs and the respective free Schiff bases. It was found that the Ag_2S nanocrystal structure and Schiff bases capping agents played a synergistic effect in the antibacterial activity, as reflected by the better biological activity of the SB-Ag_2S QDs. Based on our results and established literature we propose that the mechanism of antimicrobial activity of Schiff base-capped Ag_2S QDs can be explained by a thermally initiated electron transfer model,[8,27,28,42] providing new insight into the mode of action of their anti-pathogenic activity.

2. Experimental

2.1 Materials and reagents

Silver nitrate ($AgNO_3$), sodium sulfide ($Na_2S\cdot 9H_2O$), and thioglycolic acid ($C_2H_4O_2S$) were purchased from Sigma Aldrich. Acetylpyrazine ($C_6H_6N_2O$), 9-anthracenecarboxaldehyde ($C_{15}H_{10}O$), hydrazine hydrate (H_6N_2O), potassium hydroxide (KOH), carbon disulfide (CS_2), and other reagents of analytical grade were respectively obtained from Merck, Fluka, Alpha Chemika, and R & M Chemicals. All chemical and reagents were used as received.

2.2 Synthesis of Schiff bases

The chemical structures of Schiff bases of *S*-methyl- and *S*-benzyl-dithiocarbazate derivatives used in this study are shown in Fig. 1. The Schiff bases were synthesized based on the procedures reported by Hamid *et al.*[43] In general, hydrazine hydrate was added to a solution of KOH in ethanol, and the solution was cooled in an ice-salt bath. CS_2 was then added dropwise with constant stirring, resulting in the formation of two layers. The aqueous layer was then separated using a separating funnel, and poured into cold ethanol. Either methyl iodide or benzyl chloride was then added to the solution with vigorous stirring, giving white precipitate of the *S*-methyl- or *S*-benzyl-dithiocarbazates, respectively, which were then isolated and purified by recrystallization from absolute ethanol. The purified *S*-methyl- or *S*-benzyl-dithiocarbazates were then dissolved in hot ethanol and mixed with equimolar amounts of either 9-anthracenecarboxaldehyde or acetylpyrazine solutions to give four different Schiff bases; *i.e.* methyl (2*Z*)-2-[(anthracen-9-yl)methylidene]hydrazine-1-carbo-dithioate (**9anSM**), benzyl (2*E*)-2-[(anthracen-9-yl)methylidene]hydrazine-1-carbodithioate (**9anSB**), methyl (2*E*)-2-[1-(pyrazin-2-yl)ethylidene]hydrazine-1-carbodithioate (**AcpySM**), benzyl (2*E*)-2-[1-(pyrazin-2-yl) ethylidene]hydrazine-1-carbodithioate (**AcpySB**). The detailed syntheses and chemical characterization of the Schiff bases are described in ESI.†

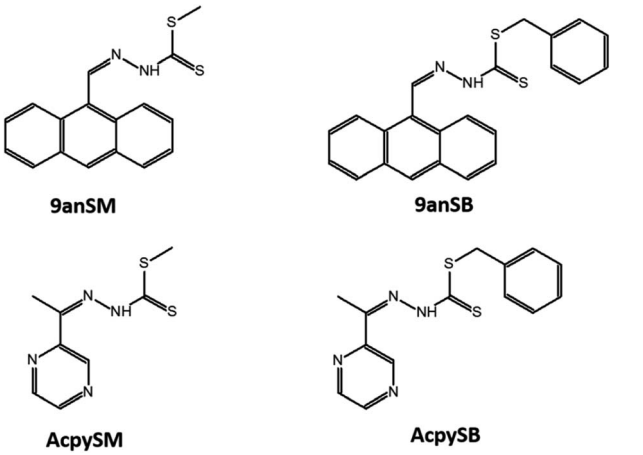

Fig. 1 The chemical structures of Schiff bases used as capping agents in this study.

2.3 Preparation of Ag_2S QDs

The SB-Ag_2S QDs were synthesized as reported by Vardar *et al.*[39] and Zhang *et al.*[44] with some modifications. 4.2×10^{-3} moles of $AgNO_3$ (0.7135 g) were dissolved 120 mL of ultrapure water in a three-necked flask under an atmosphere of nitrogen for 20 min. The pH was adjusted to 7.5 by adding NaOH and CH_3COOH to form a clear solution. 1×10^{-3} moles of each Schiff base was dissolved in 10 mL of dimethylformamide and was added to the $AgNO_3$ solution whilst stirring. The solution was then ready for the next phase. TGA-Ag_2S QDs were synthesized with a similar procedure. 5.7×10^{-3} moles of TGA (0.40 mL) were added to the $AgNO_3$ solution whilst stirring. The pH of all the mixtures was then readjusted to 7.5 to form a yellow solution. The solution was then ready for the next phase.

The next phase was the same for both SB-Ag_2S QDs and TGA-Ag_2S QDs. 2.1×10^{-3} moles of Na_2S (0.1635 g) were added to each QD solution, respectively under nitrogen bubbling, to prevent the oxidation of S^{2-}, while stirring for 20 min until a dark brown solution formed. The mixtures were then refluxed at 100 °C for 5 minutes. After cooling, the SB-Ag_2S QDs and TGA-Ag_2S QDs were isolated as a dark grey solid precipitate, and they were purified by repetitive centrifugation and washing in acetone and ultrapure water. These Ag_2S QDs were kept as an aqueous colloidal solution until use.

2.4 Measurements and characterization of Ag_2S QDs

The elemental composition of the SB-Ag_2S QDs and TGA-Ag_2S QDs were analyzed by scanning electron microscopy (SEM) combined with energy-dispersive X-ray spectroscopy (EDX) using a JSM-7600F SEM (JEOL, Japan) operating at 5.0 kV. Their shape and crystalline properties were evaluated by high resolution transmission electron microscopy (HRTEM) using an HT7830 microscope (Hitachi, Japan). Their size distributions were estimated from the TEM images.

Their electronic absorption spectra in the visible to NIR region (600–1100 nm) were recorded for dilute aqueous colloidal solutions in 1 cm cuvette on a UV-1900 spectrometer (Shimadzu, Japan). Their vibrational spectra in the range of 500–4000 cm^{-1} were measured in KBr disks on a Fourier transform infrared (FTIR) Prestige21 spectrophotometer (Shimadzu, Japan).

Their crystalline phase was determined by X-ray diffraction (XRD) measured with an angle of 2θ from 5°–80° on an Empyrean Diffractometer (PANalytical, The Netherlands) with Mo Kα radiation ($\lambda = 0.7107$ Å) under ambient condition.

2.5 Bacterial growth inhibition

The antibacterial activity of the SB-Ag_2S QDs were screened against both Gram-positive (*Bacillus subtillus* ATCC6633 and *Staphylococcus aureus* ATCC 25923) and Gram-negative (*Escherichia coli* ATCC 25922 and *Pseudomonas aeruginosa* ATCC 27853) using the agar well diffusion method, according to the Clinical Laboratory Standard Institute procedure.[45] The bacterial strains were cultured in an incubator at 37 °C for 24 h in a sterile nutrient broth (NB), which was prepared by dissolving 13.0 g of NB powder in 1 L of distilled water. Each culture (10 μL) was then diluted with 3.0 mL of NB solution to be at 0.5 McFarland standard, which was confirmed based upon its absorbance at 625 nm to be within 0.08–0.13, which is equivalent to an approximate bacterial suspension of 1.5×10^8 mL^{-1}.[46] Each bacterial culture (200 μL) was spread using a sterile glass spreader on a sterilized Muller Hinton (MH) agar plate which was prepared by pouring 25 mL of sterilised agar into a sterile Petri dish.

After drying, six wells were crafted on the agar plate with a 5 mm diameter cork borer. Into four of those wells, 40 μL of SB-Ag_2S QDs was added with an approximate concentration of 2 mg mL^{-1}, while the other two of those wells were respectively filled with similar volume and concentration of streptomycin sulfate and either DMSO or water. The streptomycin was used as a positive control, whereas DMSO or water was the negative control. Streptomycin was selected as the standard antibacterial agent because it has high solubility in water, it is naturally colourless, it is applicable to inhibit Gram-positive and Gram-negative bacterial strains, and it has a growth inhibition zone that is widely reported in the literature.[47–50] After incubation at 37 °C for 24 h, the diameter of the inhibition zone of bacterial growth on the agar plate was measured. The antibacterial screening test was repeated for at least four replicates, and the inhibition zone was calculated as the average mean value.

The MIC, which represents the lowest concentration of the SB-Ag_2S QDs that inhibited the growth of *B. subtilis*, *S. aureus*, *E. coli*, and *P. aeruginosa* bacterial strains after being incubated overnight was evaluated by preparing inoculated bacterial culture in NB to be at 0.5 McFarland standard. The standardized bacterial culture suspension was further diluted with NB solution with a ratio of 1 : 150, and was labelled as standardised inoculum. The SB-Ag_2S QDs suspensions in NB solution at different concentrations (20, 10, 5, 2.5, 1.25, 0.625, 0.313, 0.156, 0.0781, and 0.0392 mg mL^{-1}) were prepared in 96-well plates by 2-fold dilutions. All the suspensions (50 μL) were then mixed with the same volume of the standardised inoculum, and the mixtures were then incubated at 37 °C overnight.

The MBC of the SB-Ag_2S QDs was investigated against *S. aureus*, bacterial strain by observing the lowest concentration which showed no bacterial growth observable on the MH agar plates. In this test, 200 μL of MH agar was poured into the Petri dish. The agar plates were divided into 4 sections, which could be considered as replications. Once the agar had solidified, a sterile inoculating loop was inserted into the test tubes containing SB-Ag_2S QDs and was swabbed onto the surface of the solidified agar. After overnight incubation at 37 °C, the bacterial growth was assessed, and the samples which showed no visible bacterial growth were taken to represent the MBC.[51]

The bacterial growth inhibitions of TGA-Ag_2S QDs and the four free Schiff bases used in this study were tested against the same bacterial strains under the same experimental conditions. The diameter of the inhibition zone was recorded, and was compared with those of the SB-Ag_2S QDs.

2.6 Fungal growth inhibition

The antifungal activities of the four SB-Ag_2S QDs were examined using the agar well diffusion method against colony formation of *Candida albicans* (ATCC 40042), according to the Clinical Laboratory Standard Institute procedure.[45] The fungal cultures were cultivated by inoculating 100 μL of fungal stock culture in 5 mL of NB and these were left incubated in a water bath at 37 °C and agitated at 150 rpm. A cloudy fungal culture was observed after 48 hours, indicating successful fungal growth. The fungal culture was then diluted using NB to ensure that it is equivalent to 0.5 McFarland standard. 200 μL of the standardised culture was poured and homogenized on MHA plates using a sterile spreader and allowed to dry for a few minutes. Six wells were then made in each MHA plate using a 0.5 cm diameter cork borer. Into five of those wells, 40 μL of SB-Ag_2S QDs was gently pipetted with an approximate concentration of

2 mg mL^{-1}, and 40 μL of ultrapure water was pipetted into the sixth well as a negative control. The agar plates were then incubated at 37 °C for 48 hours. Finally, the measurement for the diameter of inhibition zone where there is no fungal growth observed was recorded. The data was collated by taking the mean of the replicates of each sample. The fungal growth inhibitions of TGA-Ag_2S QDs and the four free Schiff bases were performed under the same experimental condition. The diameter of the inhibition zone was recorded, and was compared with those of the SB-Ag_2S QDs.

2.7 Brine shrimp lethality bioassay

The toxicity of SB-Ag_2S QDs was established by employing a shrimp lethality bioassay which was performed in 12-well plate. Brine shrimp larvae (*Artemia nauplii* L.) were prepared by hatching the shrimp eggs at 30 °C for 2 days in a shallow rectangular container containing artificial seawater. Ten brine shrimp larvae were collected from the hatching container, and were transferred into each well of triplicate plates, followed by the addition of 0.5 mL aliquots of the QDs samples with different concentrations (100, 10, 1 and 0.1 mg mL^{-1}). 0.5 mL of the artificial seawater was used as a negative control. Each well was further adjusted by adding 4.5 mL of artificial seawater, thus the final concentrations of QDs in each well were (10 000, 1000, 100, and 10 μg mL^{-1}, respectively). The plates were then incubated under illumination at 25–30 °C. After incubation for 24 h, the number of surviving shrimp larvae was recorded. The average percentage lethality was plotted as a function of the logarithm of the QD concentration. The toxicity is defined by the LC_{50} which is the lethal concentration killing 50% of the larvae.

3. Results and discussion

3.1 The formation of Schiff bases-Ag_2S QDs

The formation of SB-Ag_2S QDs and TGA-Ag_2S QDs was confirmed from their characterization data, including visible NIR absorption and FTIR spectra, EDX and XRD, and TEM imaging. Fig. 2 shows the visible-NIR absorption spectra of SB-Ag_2S QDs and TGA-Ag_2S QDs grown at 100 °C for 5 min. The spectra consisted of a baseline rising towards shorter wavelength resulting from elastic Rayleigh scattering and a narrow absorption band at 970 nm assigned to the lowest optical transition of Ag_2S QDs as reported by Christy *et al.*[52] However, the peak maximum was at slightly shorter wavelength compared to that reported by Sun *et al.* (1010 nm).[53] The absorption bands of SB below 500 nm (Fig. S1†) were not present, because the number of molecules on the surface is too low for their absorption to register above the Rayleigh scattering. The spectra had similar peak maxima, indicating that the particle sizes of the Ag_2S QDs are also similar.

The FTIR spectra of SB-Ag_2S QDs are shown in Fig. 3, while the spectra of their respective Schiff bases are shown in Fig. S2.† The FTIR spectra of Ag_2S QDs showed the characteristic Ag–S and Ag–N vibrations at 420–600 cm^{-1}.[54] The broad band at 3450 cm^{-1} and shoulder band at 1600 cm^{-1} are assigned to the

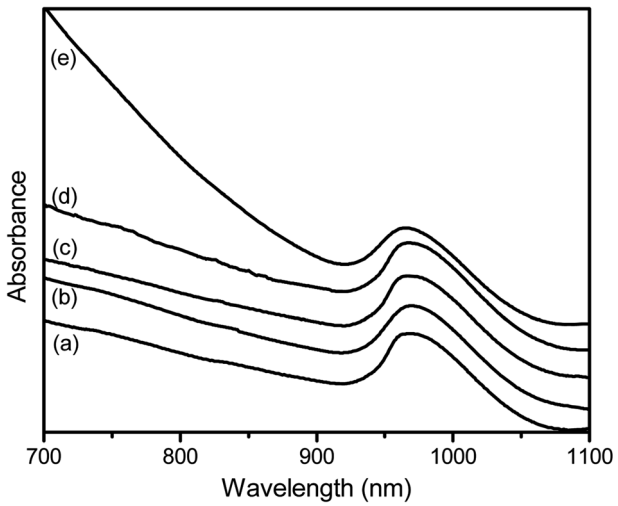

Fig. 2 The Vis-NIR spectra of (a) **9anSM**-Ag_2S (b) **9anSB**-Ag_2S, (c) **AcpySM**-Ag_2S, (d) **AcpySB**-Ag_2S, and (e) TGA-Ag_2S QDs grown at 100 °C for 5 min.

OH stretching and bending vibrational modes of residual water adsorbed onto the Ag_2S QDs surface.[55] The main vibrational bands at 3080, 2857, 1627, 1552, 956, 735 cm^{-1} are assigned to the Schiff bases (N–H, C–H, C=N, C=C aromatics, C=S, and C–S stretching vibrations, respectively).[56,57] It is noteworthy that several of the Schiff base's vibrational bands of the SB-Ag_2S QDs were shifted to lower frequency or their intensities were suppressed compared to those of the respective free Schiff bases, indicating less electron delocalisation, which is most likely due to the interaction of the thione (–C=S) and imine (–C=N–) moieties to Ag_2S.

The FTIR spectrum of TGA-Ag_2S QDs (Fig. 2(e)) showed no S–H vibrational band, which is typically observed at ~2560 cm^{-1}, indicating that the TGA coordinates through the thiol group.[30,58] As was the case for SB-Ag_2S QD, strong bands at 3450 and 1600 cm^{-1} are also attributed to the vibrations of

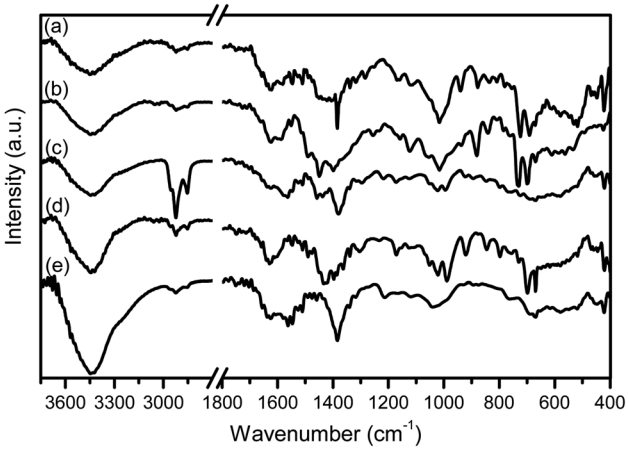

Fig. 3 The FTIR spectra of (a) **9anSM**-Ag_2S, (b) **9anSB**-Ag_2S, (c) **AcpySM**-Ag_2S, (d) **AcpySB**-Ag_2S, and (e) TGA-Ag_2S QDs grown at 100 °C for 5 min.

adsorbed water molecules. Importantly, the Ag–S vibration consistently appeared as a broad band at 420–600 cm^{-1}.

From the SEM images of SB-Ag_2S QDs prepared using the colloidal method shown in Fig. S3,† they can be seen to form irregular agglomerates. The particles in the agglomerates were mostly spheroidal with a rough surface morphology. The sizes and surface morphology of agglomerated SB-Ag_2S QDs were similar to those of TGA-capped Ag_2S QDs. The SEM-EDX identified and quantified the elements present in the SB-Ag_2S and TGA-Ag_2S QDs. As shown in Fig. S3,† the EDX spectrum verified the presence of the elements Ag and S in SB-Ag_2S QDs with atomic percentage ratio of Ag and S being 54.3 : 27.4, which equates to approximately 2 to 1, confirming the Ag_2S formation. A similar approximate atomic percentage ratio of Ag and S was also found in TGA-capped Ag_2S QDs. It is noted that there is a slightly higher atomic percentage of S in the SB-Ag_2S QDs which may come from the Schiff bases on the QDs surface.

The HRTEM images of **AcpySB**-Ag_2S QDs and TGA-Ag_2S QDs along with their particle size distribution are shown in Fig. 4, as typical representative examples. Those of **9anSM**-, **9anSB**-, and **AcpySM**-Ag_2S QDs are presented in Fig. S4.† The HRTEM images demonstrated that the QDs were nearly spherical and had high crystallinity as seen by their clear lattice fringes.

Based on the TEM images, the particle size distribution of the SB-Ag_2S QDs was obtained by estimating the diameter of at least 70 particles. The size ranges were 5.6 ± 2.2 nm, 4.8 ± 1.7 nm, 5.0 ± 2.1 nm, and 4.0 ± 1.3 nm, for **AcpySB**-Ag_2S, **9anSM**-Ag_2S, **9anSB**-Ag_2S, and **AcpySM**-Ag_2S QDs, respectively. The size range of the TGA-Ag_2S QDs was 6.3 ± 2.4 nm. This confirms that the SB-Ag_2S QDs are slightly smaller compared to TGA-Ag_2S QDs in this study and those reported by Wang *et al.* (6.98 nm),[59] and Sun *et al.* (9.0 nm).[53] These results explain the shorter wavelength peak maximum of the NIR absorption band for the SB-Ag_2S QDs compared to those previously reported for bovine serum albumin (BSA)-Ag_2S QDs[59] and TGA-Ag_2S QDs.[53] Since the particle sizes of the SB-Ag_2S QDs are only slightly larger than the Ag_2S exciton diameter (in the range of 3.0–4.4 nm),[60] one can expect that these Ag_2S QDs have a strong quantum confinement effect.

The crystallinity and crystalline phase of the SB-Ag_2S TGA-Ag_2S QDs was established using XRD. As shown in Fig. 5, the XRD patterns have diffraction peaks at 26.4°, 29.0°, 31.6°, 33.7°, 34.5°, 34.9°, 36.8°, 37.8°, 40.7°, 43.5°, 45.6°, 46.4°, 48.0°, 48.9°, 53.3° which faithfully match the expected positions of the (−112), (110), (−113), (−121), (−122), (013), (−104), (031), (−202) (−212), (112), (−214), (014), (−224) planes of monoclinic phase α-Ag_2S (acanthite; space group no. 14, $P2_1/c$).[61] Based on the XRD patterns, the lattice fringe spacing (d) observed in the TEM image (Fig. 4) was estimated using the relation $d = \lambda/2 \sin\theta$; (where λ is the incident X-ray wavelength and θ is the Bragg diffraction angle) and was found to be 0.119 nm, which corresponds to the (−112) facet of the acanthite Ag_2S.

The large width of the diffraction peaks is a result of the small crystallite sized Ag_2S nanocrystals.[62] The profile of diffraction band at 34.5°, which had the highest diffraction intensity, was used to estimate the average crystallite size (D) of the Ag_2S QDs using the Scherrer formula;[63]

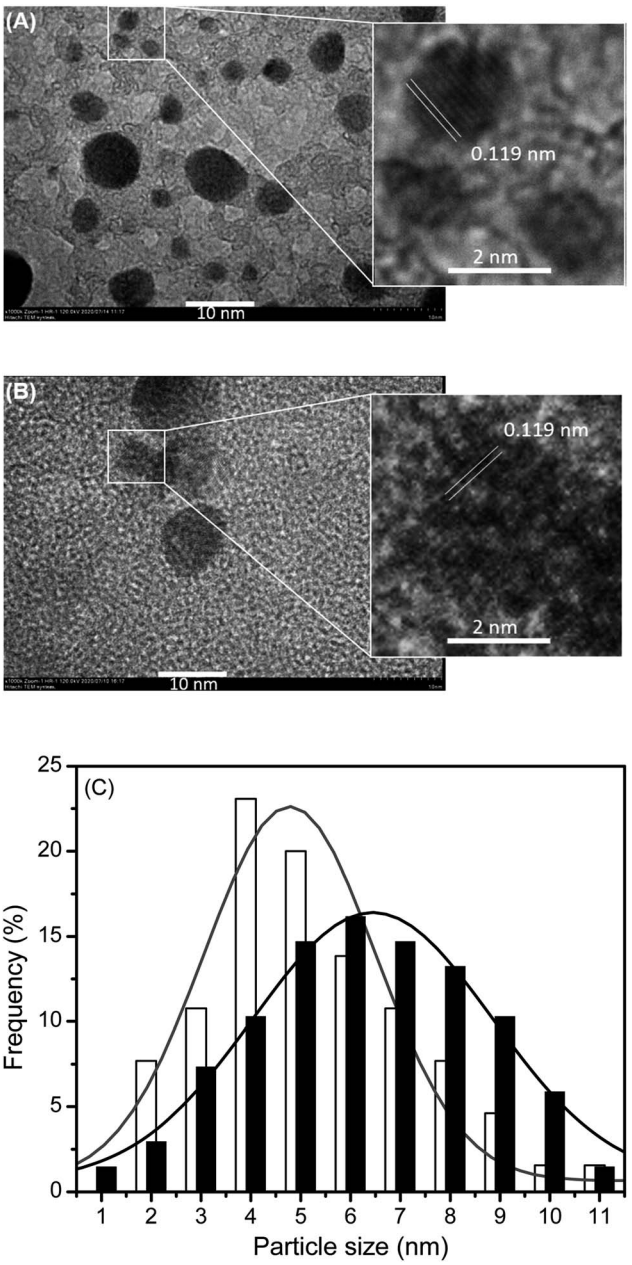

Fig. 4 The HRTEM images of (A) **AcpySB**-Ag_2S QDs and (B) TGA-Ag_2S QDs, showing their lattice fringes with spacing of 0.119 nm, corresponding to the (−112) plane of acanthite Ag_2S, and (C) the particle size distribution of **AcpySB**-Ag_2S QDs (white bars) and TGA-Ag_2S QDs (black bars) along with their respective best-fit Gaussian curve.

$$D = \kappa\lambda/\beta(\cos\theta)$$

where κ is the Scherrer constant (0.9) and β is the full width at half-maximum of the Bragg diffraction peak. The average crystallite size of the SB-Ag_2S and TGA-Ag_2S QDs was calculated to be 5.1 and 5.8 nm, respectively, which is in good agreement with the sizes determined from TEM images (see Fig. 4), suggesting that the QDs consisted of a single crystalline structure.

The above findings are consistent with the Schiff bases being complexed with Ag^+, followed by the formation of Ag_2S salts

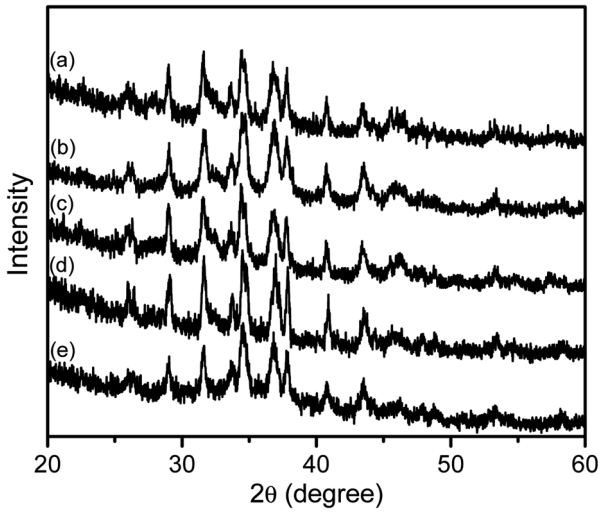

Fig. 5 The XRD patterns of (a) **9anSM**-Ag_2S, (b) **9anSB**-Ag_2S, (c) **AcpySM**-Ag_2S, (d) **AcpySB**-Ag_2S, and (e) TGA-Ag_2S QDs grown at 100 °C for 5 min.

which were aggregated, leading to the formation of SB-Ag_2S QDs, as schematically illustrated in Scheme 1. A similar reaction mechanism for Ag_2S QDs has been reported by Jiang *et al.*[10] and Siva *et al.*[64] respectively using 3-mercaptopropionic acid (3-MPA) and L-cysteine as capping agents. This indicates that, in general, the mechanism of the bottom-up synthetic approach of QDs involves similar elementary steps, including the interaction between the metallic cation with the capping agent, followed by the formation of Ag_2S salts which then crystallize to form the nanocrystals.[65] It is important to recall that the particle sizes of SB-Ag_2S QDs were slightly smaller compared to TGA-Ag_2S QDs, most probably due to the larger molecular sizes of the Schiff bases compared to TGA, which should inhibit the growth of the QDs preventing them from developing into larger-sized particles.

These findings confirm that SB-Ag_2S QDs have been successfully synthesized by a facile one-pot synthesis method, implying that the SBs could chelate Ag^+ and that the complexes were further neutralized by S^{-} ions and crystallized to form SB-Ag_2S QDs. The formation, crystal structure, and physical characteristics of these Ag_2S QDs capped with Schiff base ligands synthesized by the one-pot synthesis method are similar to those of other Ag_2S QDs capped with BSA,[59] TGA,[53] 2-MPA,[30] 3-MPA,[10] D-penicillamine,[31] alkyl,[3] 2-(benzylidene amino)benzothiol,[37] and EDTA[38] prepared *via* one-pot synthesis, one-pot microwave assisted reaction, pyrolysis, chemical condensation, solvothermal, and hydrochemical bath deposition methods. Nevertheless, the particle sizes of SB-Ag_2S QDs (4.0–5.6 nm) synthesized by our one-pot synthesis tend to be smaller as compared those Ag_2S QDs prepared with the other methods, such as alkyl-Ag_2S QDs (10.2 nm) *via* pyrolysis,[3] 2-(benzylidene amino) benzothiol-Ag_2S QDs (42 nm) *via* solvothermal,[37] and EDTA-Ag_2S QDs (10–20 nm) *via* hydrochemical bath deposition.[38] This means that the one-pot synthesis is an effective method for producing smaller size-controlled Ag_2S QDs.

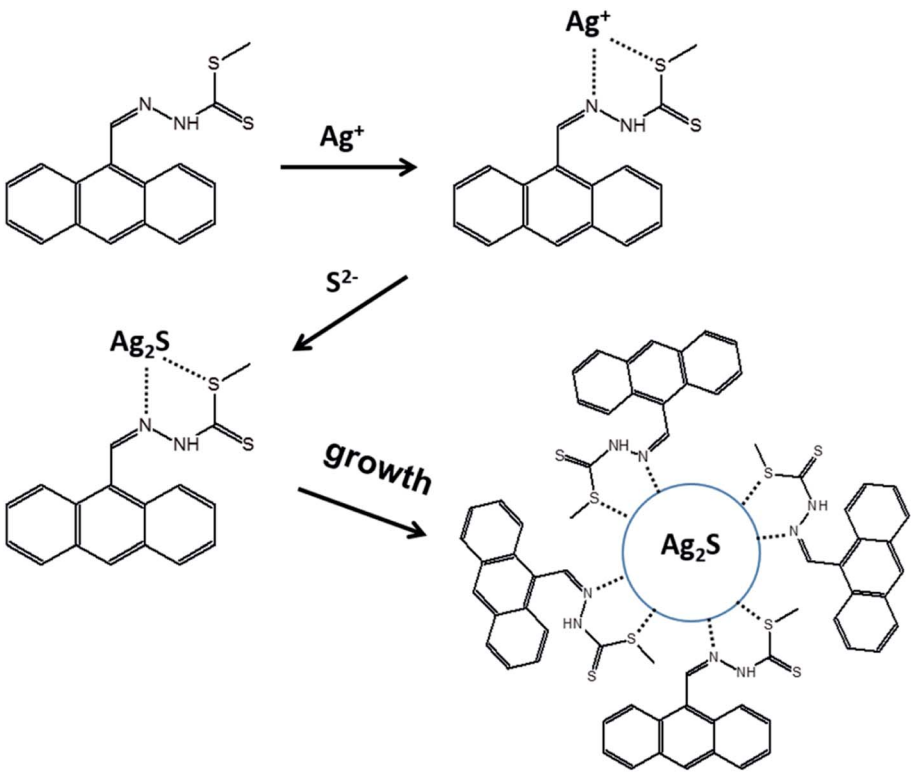

Scheme 1 Schematic illustration the mechanism of the formation of **9anSM**-Ag_2S QDs, as a representative example of the general formation mechanism proposed for SB-Ag_2S QDs.

3.2 Antibacterial and antifungal activities

The disk diffusion assay results suggested that the SB-Ag_2S QDs exhibited good antibacterial activities against both Gram-positive (*B. subtilis* and *S. aureus*) and Gram-negative (*E. coli* and *P. aeruginosa*) bacterial strains, with various diameters of inhibition zones, as summarized in Table 1, while the representative images of growth inhibition zones of *B. subtilis* nurtured with Schiff base-Ag_2S QDs are given in Fig. S6.† This is a qualitative indication that the SB-Ag_2S QDs have antibacterial activities regardless of the thickness of the peptidoglycan layer or the presence of an outer lipid membrane on the bacterial cells. However, the bacterial growth inhibition zones of the SB-Ag_2S QDs were approximately two-thirds smaller than those of streptomycin sulfate, suggesting that they have lower antibacterial activities.

Using the same antibacterial screening procedures, the antibacterial activities of the SB-Ag_2S QDs were also compared with those of the respective free Schiff bases and the TGA-Ag_2S QDs. In general, except for **AcpySM**, all the Schiff bases in this study and the TGA-Ag_2S QDs were inactive against the Gram-positive and Gram-negative bacteria. This clearly shows that the antibacterial activities of SB-Ag_2S QDs is a function of the capping agents. It might further indicate that the Schiff bases on the QDs are more polarised enhancing their interaction with the bacterial cell membrane.

The MIC of the SB-Ag_2S QDs toward the Gram-positive and Gram-negative bacterial strains were in the range of 5–75 μg mL^{-1}, as summarised in Table 2, demonstrating that only low concentrations of the Ag_2S QDs are required to inhibit the bacterial growth. It is important to highlight that all of the SB-Ag_2S QDs had an MIC value of 5–10 μg mL^{-1} toward *B. subtilis* bacterium. Representative images of the microbroth dilution method to determine the MIC of Schiff base-Ag_2S QDs to inhibit *B. subtilis* are presented in Fig. S7.† Those of streptomycin and TGA-Ag_2S QDs are also presented for comparison. These MIC values were even lower or at least comparable to streptomycin (10 μg mL^{-1}).[47] In particular, **9anSB**- and **AcpySM**-Ag_2S QDs have MIC values in the range of 5–11 μg mL^{-1} toward *E. coli* bacterium, which is much lower than that of streptomycin (25 μg mL^{-1}),[48] whereas the MIC value of **9anSM**-Ag_2S QDs toward *P. aeruginosa* bacterium was 6 μg mL^{-1}, which is also lower than streptomycin (8 μg mL^{-1}).[49] These results show that in certain screening assays the SB-Ag_2S QDs exhibit even stronger antibacterial activity than streptomycin.

The capability of SB-Ag_2S QDs to act as antibacterial agents were further confirmed by the susceptibility of Gram-positive, *S. aureus* bacterium. As summarised in Table 2, the MBC of **9anSM**- and **AcpySM**-Ag_2S QDs were 125 and 250 μg mL^{-1}, respectively, while those of **9anSB**- and **AcpySB**-Ag_2S QDs were 800 μg mL^{-1}. In comparison, the MBC of streptomycin sulfate against *S. aureus* has been reported to be in the range between 12 to 18 μg mL^{-1}.[50] Based on these MBC values, the Ag_2S QDs capped with Schiff bases of *S*-methyl-dithiocarbazate derivatives could be considered as bactericidal agents, while those capped with *S*-benzyl-dithiocarbazate derivatives were bacteriostatic agents or bacterial inhibitors.[51] These results highlight that the potential to apply SB-Ag_2S QDs as new antibacterial agents, causing either bacteriostatic or bactericidal impact where the growth of the bacterial growth is inhibited or the bacteria is even killed.[66]

The SB-Ag_2S QDs exhibit antifungal activity against *C. albicans*. The mean diameter of inhibition zone of the Schiff bases-Ag_2S QDs was 11.4–13.6 mm, as shown in Table 1. The inhibition zones of *C. albicans* nurtured with Schiff base-Ag_2S QDs are shown in Fig. S8.† In contrast, TGA-Ag_2S QDs and the corresponding free Schiff bases have no detectable antifungal activity. In comparison, the sizes of the inhibition zone of the SB-Ag_2S QDs against *C. albicans* was slightly larger than those of Ag/In/S QDs (9.5–10 mm).[67] It is likely that the Schiff bases, when attached to the surface of Ag_2S QDs, can interact with the fungus cell surface damaging the cell wall resulting in either cell growth inhibition or even penetration of the Ag_2S QDs into the cell due to the permeability of the fungus cell wall. As explained above, this could induce oxidative stress in the cells, which would eventually result in the inhibition of cell growth and even cell death, as described in the literature.[68,69]

The MIC of the SB-Ag_2S QDs against *C. albicans* were in the range of 40–310 μg mL^{-1}, as summarised in Table 2. Images of

Table 1 The comparison of the inhibition zones of Gram-positive and Gram-negative bacterial strains and fungus by Schiff bases-Ag_2S QDs and TGA-Ag_2S QDs along with the standard streptomycin[a]

		Inhibition zone (mm)				
Sample		*B. subtilis*	*S. aureus*	*E. coli*	*P. aeruginosa*	*C. albicans*
Schiff bases-Ag_2S QDs	**9anSM**-Ag_2S	13.5 ± 0.8	13.8 ± 1.1	13.8 ± 1.2	12.3 ± 1.9	13.6 ± 0.8
	9anSB-Ag_2S	12.0 ± 1.0	9.8 ± 0.8	ND	10.5 ± 1.1	11.4 ± 0.9
	AcpySM-Ag_2S	12.3 ± 1.3	15.0 ± 2.0	11.0 ± 1.7	14.5 ± 0.7	13.6 ± 0.9
	AcpySB-Ag_2S	11.8 ± 0.7	ND	ND	10.8 ± 1.2	12.8 ± 0.5
Schiff bases	**9anSM**	ND	ND	ND	ND	ND
	9anSB	ND	ND	ND	ND	ND
	AcpySM	11.5 ± 1.5	9.0 ± 1.9	8.3 ± 1.3	ND	ND
	AcpySB	ND	ND	ND	ND	ND
TGA-Ag_2S QDs		ND	ND	ND	ND	ND
Streptomycin		21.3 ± 1.7	21.0 ± 2.9	21.5 ± 1.9	19.0 ± 2.1	—

[a] ND denotes that no bacterial growth inhibition was detected.

Table 2 The of MIC values for Schiff bases-Ag_2S QDs and streptomycin for comparison

Sample		MIC (μg mL^{-1})					MBC (μg mL^{-1})
		B. subtilis	*S. aureus*	*E. coli*	*P. aeruginosa*	*C. albicans*	*S. aureus*
Schiff bases-Ag_2S QDs	**9anSM**-Ag_2S	5	20	70	6	80	125
	9anSB-Ag_2S	5	10	5	10	40	800
	AcpySM-Ag_2S	10	20	11	14	310	250
	AcpySB-Ag_2S	5	10	50	10	310	800
Streptomycin		10 (ref. 47)	10 (ref. 47)	25 (ref. 48)	8 (ref. 49)	—	12–18 (ref. 50)

the results from the microbroth method to determine the MIC of *C. albicans* nurtured with Schiff base-Ag_2S QDs are shown in Fig. S8.† The lowest MIC was seen for **9anSB**-Ag_2S QDs, followed by **9anSM**-Ag_2S, **AcpySM**-Ag_2S, and **AcpySB**-Ag_2S QDs. It is notable that the MIC of the SB-Ag_2S QDs were much higher than that of other Ag nanoparticles (1–7 μg mL^{-1}),[70] but much lower compared with ibuprofen (2048 μg mL^{-1}).[71] This result confirms that the SB-Ag_2S QDs also act as antifungal agent and inhibit fungal growth.

Antibacterial and antifungal mechanism of functionalized QDs and low-dimensional materials have been summarized by Rajendiran *et al.*[68] and Shaw *et al.*[72] It has been pointed out that the most commonly proposed antimicrobial mechanism of QDs involves chemical interferences and oxidative stress, leading to membrane damage, protein dysfunction, nucleic acid fragmentation, and transcriptional arrest.[73] In particular, the QDs interact with the phospholipid layer of bacterial membranes, and metallic ions on their surface disrupt the cell respiration and cellular pathways.[74] The oxidative stress due to intracellular reactive oxygen species generated upon interaction between the QDs with the bacterial cells disrupts phospholipids, nucleic acids, proteins, resulting in cell lysis.[75] Surface chemical functionalisation is considered to enhance the production of reactive oxygen species, destroying the cell wall, and disrupting nucleic acids.[76] In this sense, one could consider the QDs functionalized with highly π-conjugated compounds would accelerate charge separation and the production of reactive oxygen species.[72] Taking this into account, one possible mechanism for the antimicrobial action is that there is an interaction between the Schiff bases on the Ag_2S QDs surface and the bacterial cell wall or cell membrane which creates oxidative stress and damage the cell wall, leading to cell rupture.[77,78] This proposed interaction of the QD-bound Schiff bases and the bacterial cells is supported by the fact that there should be an electrostatic attraction between the positively charged QDs and the negatively charged phospholipid bilayer of the bacterial cell.[77,78] It has also been proposed that metal oxide QDs can transfer an electron into the bacterial cell or produce reactive oxygen species (ROS), increasing cytotoxicity by producing reactive oxygen species within the cell, which would inhibit metabolic processes and kill the cell,[77–79] and this would also apply to SB-Ag_2S QDs. In this sense, a synergistic cooperative effect between the Schiff bases and the Ag_2S core is proposed for the antibacterial activities of SB-Ag_2S QDs. The Schiff bases are highly conjugated across the entire molecule, whereas TGA is not. Therefore, the conjugated electron clouds on the Schiff bases should facilitate electron transfer to the pathogen cell walls, whereas the unconjugated TGA would insulate the Ag_2S core preventing electron transfer.

The electron transfer mechanism is proposed based on the possibility of dark (thermalized) electron transfer from Ag_2S to the Schiff's base and to the cell wall. The principle reason for our argument is that, Fermi levels in Ag_2S is 10 eV, with a bandgap of ∼1 eV.[8] The Ag_2S band gap can be exceeded, and the conduction band can be populated at room temperature.[42] Furthermore, it is well understood that π-conjugated molecules such as Schiff bases have a higher HOMO energy levels and a lower LUMO energy levels, which would facilitate more efficient electron hopping (transfer) from the Ag_2S to the Schiff bases LUMO. The energy of the LUMO level should generally follow the trend of the degree of conjugation. Consequently, if our proposed mechanism is reasonable, the antibacterial and antifungal activity should generally follow the same trend, which indeed it is demonstrated in this study.

We may also recall that Ag_2S conduction band is similar in energy to a typical organic dye's excited state or even higher.[27,28] Therefore, a thermally excited electron hopping from the Ag_2S conduction band through the organic dye's excited state (LUMO) is not only feasible in terms of the energetics of the system but it is very likely to happen. Nevertheless, we do not rule out electron transfer from the Fermi level, if the LUMO of the dye is lower in energy than the Fermi level. Therefore, attaching Schiff bases as capping agents is not just the conjugation providing a "conducting" bridge between the Ag_2S and the cell wall, it is the relative LUMO energies of the Schiff bases with respect to the Ag_2S conduction band and Fermi level that would be important. Once inside the Schiff base LUMO, the electron can further interact with the typical electron acceptors in the cell wall, as well as with water in the medium to produce ROS, which are well established as precursors that produce cell death in dark (non-light-initiated) reactions.[77]

3.3 Toxicity test

The results of toxicity of SB-Ag_2S QDs against *A. nauplii* shrimp larvae are presented in Table S1.† Based on a total larvae number of 360 from triplicates, at the concentrations of SB-Ag_2S QDs of 10 000, 1000, 100, and 10 μg mL^{-1}, the average larval deaths were found to be in the range of 0 to 40%. At the lowest QD concentration of 10 μg mL^{-1} the mortality of larvae in the presence of the Ag_2S QDs was 0%, except for **AcpySB**-Ag_2S QDs

which induced larval mortality of 3.3%. The mortality of larvae increased with QDs concentration, and in the highest QDs concentration of 10 000 μg mL^{-1}, the mortality was in the range of 5.1–39.5%, revealing that among the SB-Ag_2S QDs, **AcpySB**-Ag_2S QDs was the most toxic, followed by **9anSB**-, **AcpySM**-, and then the **9anSM**-Ag_2S QDs. In comparison, TGA-Ag_2S QDs even in its highest concentration showed mortality of larvae of less than 3%. It is notable that LC_{50} values of SB-Ag_2S QDs were more than 1000 μg mL^{-1}, suggesting that the SB-Ag_2S QDs were not toxic to *A. nauplii* shrimp.[80]

4. Conclusions

Ag_2S QDs have been made in a one-pot synthesis. In this study, for the first time, four different Schiff bases of *S*-methyl- or *S*-benzyl-dithiocarbazate derivatives have been used as stabilizing agents. The SB-Ag_2S QDs were nearly spherical with average sizes being in the range of 4.0 nm to 5.6 nm, which is smaller compared to conventional thioglycolic acid (TGA)-capped Ag_2S QDs. It was confirmed that the SB-Ag_2S QDs had good antibacterial activities against Gram-positive and Gram-negative bacterial strains as well as antifungal activities against *C. albicans*. This was in contrast to the biologically inactive or low activity TGA capped Ag_2S QDs and respective free Schiff bases. It is therefore concluded that the bioactivities of the SB-Ag_2S QDs is a function of the cooperative interaction between Schiff bases as capping agents, which enhances an electrostatic attraction between the positively charged QDs with the negatively charged phospholipid bilayer of the bacterial cell wall and glucans and glycoproteins of fungus cell wall, destroying the membrane cell walls. The MIC results confirmed that it only required low concentrations of the SB-Ag_2S QDs to inhibit the growth *B. subtillus*, *E. coli*, and *P. aeruginosa* bacterial strains as well as *C. albicans*, which were to some extent comparable or lower than those of streptomycin and ibuprofen. This confirms their strong capacity to inhibit bacterial and fungal growth. The Ag_2S QDs capped with Schiff bases of *S*-methyl-dithiocarbazate derivatives could be considered as bactericidal agents, while those capped with *S*-benzyl-dithiocarbazate derivatives were bacteriostatic agents or bacterial inhibitors. Overall, this study reports novel functionalized Ag_2S QDs using Schiff bases as capping agents for antimicrobial applications. The conjugated electron clouds on the Schiff bases should facilitate electron transfer to the pathogen cell walls, whereas the unconjugated TGA would insulate the Ag_2S core preventing electron transfer. Results of lethality assay revealed that SB-Ag_2S QDs were not toxic to brine shrimp (*Artemia salina*). The investigation on antiamoebic and anticancer activities are of further interest to explore as other possible biological applications of these novel SB-Ag_2S QDs.

Author statement

N.·N. M. Shahri performed the experiments. H. Taha analysed the antibacterial activity. M. H. S. A. Hamid facilitated the syntheses of Schiff bases. E. Kusrini analysed XRD data, J.-W. Lim analysed HRTEM data, J. Hobley analysed data and reviewed the manuscript, and A. Usman conceived the project and wrote the manuscript.

Conflicts of interest

There are no conflicts to declare.

Acknowledgements

The authors would like to acknowledge Elena Babai@Endru for her assistance in the early stages of MIC analysis. EK is grateful to Universitas Indonesia for PUTI Q1 Research Grant No: NKB-4036/UN2.RST/HKP.05.00/2020. JH is grateful to NCKU90 for providing his Distinguished Visiting Scientist position.

References

1 C. T. Matea, T. Mocan, F. Tabaran, T. Pop, O. Mosteanu, C. Puia, C. Iancu and L. Mocan, *Int. J. Nanomed.*, 2017, **12**, 5421–5431.
2 K. Xiong, J. Li, L. Tan, Z. Cui, Z. Li, S. Wu, Y. Liang, S. Zhu and X. Liu, *Colloid Interface Sci. Commun.*, 2019, **33**, 100201.
3 Y. Du, B. Xu, M. Cai, F. Li, Y. Zhang and Q. Wang, *J. Am. Chem. Soc.*, 2010, **132**, 1470–1471.
4 I. G. Theodorou, Z. A. R. Jawad, H. Qin, E. O. Aboagye, A. E. Porter, M. P. Ryan and F. Xie, *Nanoscale*, 2016, **8**, 12869–12873.
5 K. Akamatsu, S. Takei, M. Mizuhata, A. Kajinami, S. Deki, S. Takeoka, M. Fujii, S. Hayashi and K. Yamamoto, *Thin Solid Films*, 2000, **359**, 55–60.
6 J. Xue, J. Liu, S. Mao, Y. Wang, W. Shen, W. Wang, L. Huang, H. Li and J. Tang, *Mater. Res. Bull.*, 2018, **106**, 113–123.
7 D. Aydemir, M. Hashemkhani, H. Y. Acar and N. N. Ulusu, *Mol. Biol. Rep.*, 2020, **47**, 4117–4129.
8 S. Kashida, N. Watanabe, T. Hasegawa, H. Iida, M. Mori and S. Savrasov, *Solid State Ionics*, 2003, **158**, 167–175.
9 K.-Y. Yong, I. Roy, H. Ding, E. J. Bergey and P. N. Prasad, *Small*, 2009, **5**, 1997–2004.
10 P. Jiang, C.-N. Zhu, Z.-L. Zhang, Z.-Q. Tian and D.-W. Pang, *Biomaterials*, 2012, **33**, 5130–5135.
11 G. Hong, J. T. Robinson, Y. Zhang, S. Diao, A. L. Antaris, Q. Wang and H. Dai, *Angew. Chem., Int. Ed. Engl.*, 2012, **51**, 9818–9821.
12 F. D. Duman, I. Hocaoglu, D. G. Ozturk, D. Gazuacik, A. Kiraz and H. Y. Acar, *Nanoscale*, 2015, **7**, 11352–11362.
13 O. Bruns, T. Bischof, D. Harris, D. Franke, Y. Shi, L. Riedemann, A. Bartelt, F. B. Jaworski, J. A. Carr, C. J. Rowlands, M. W. B. Wilson, O. Chen, H. Wei, G. Hwang, D. M. Montana, I. Coropceanu, O. B. Achorn, J. Kloepper, J. Heeren, P. T. C. So, D. Fukumura, K. F. Jensen, R. K. Jain and M. G. Bawendi, *Nat. Biomed. Eng.*, 2017, **1**, 0056.
14 B. Purushothaman and J. M. Song, *Biomater. Sci.*, 2021, **9**, 51–69.
15 D. Bera, L. Qian, T. K. Tseng and P. H. Holloway, *Materials*, 2010, **3**, 2260–2345.

16 E. Navarrete, V. Rojas, M. Romero, J. Román, G. Cáceres, R. Henríquez, P. Grez, R. Schrebler, F. Herrera and E. Muñoz, *J. Solid State Electrochem.*, 2021, **25**, 133–140.
17 A. Mansur, H. Mansur and J. González, *Sensors*, 2011, **11**, 9951–9972.
18 Z. Y. Chen, H. N. Abdelhamid and H. F. Wu, *Rapid Commun. Mass Spectrom.*, 2016, **30**, 1403–1412.
19 B. R. Singh, S. Dwivedi, A. A. Al-Khedhairy and J. Musarrat, *Colloids Surf., B*, 2011, **85**, 207–213.
20 K. Shivaji, S. Mani, P. Ponmurugan, C. S. De Castro, M. L. Davies, M. G. Balasubramanian and S. Pitchaimuthu, *ACS Appl. Nano Mater.*, 2018, **1**, 1683–1693.
21 S. A. Matar, W. H. Talib, M. S. Mustafa, M. S. Mubarak and M. A. AlDamen, *Arabian J. Chem.*, 2015, **8**, 850–857.
22 E. Yousif, A. Majeed, K. Al-Sammarae, N. Salih, J. Salimon and B. Abdullah, *Arabian J. Chem.*, 2017, **10**, 1639–1644.
23 C. M. da Silva, D. L. da Silva, L. V. Modolo, R. B. Alves, M. A. de Resende, C. V. B. Martins and Â. Fátima, *J. Adv. Res.*, 2011, **2**, 1–8.
24 K. M. Khan, N. Ambreen, A. Karim, S. Saied, A. Amyn, A. Ahmed and S. Perveen, *J. Pharmacol. Res.*, 2012, **5**, 651–656.
25 S. Murtaza, M. S. Akhtar, F. Kanwal, A. Abbas, S. Ashiq and S. Shamim, *J. Saudi Chem. Soc.*, 2017, **21**, S359–S372.
26 G. Matela, *Adv. Anticancer Agents Med. Chem.*, 2020, **20**, 1908–1917.
27 C. Chen, Z. Li, H. Lin, G. Wang, J. Liao, M. Li, S. Lv and W. Li, *Dalton Trans.*, 2016, **45**, 3750–3758.
28 L. Cheng, H. Ding, C. Chen and N. Wang, *J. Mater. Sci.: Mater. Electron.*, 2016, **27**, 3234–3239.
29 N. S. Kozhevnikova, A. S. Vorokh, E. V. Shalaeva, I. V. Baklanova, A. P. Tyutyunnik, V. G. Zubkov, A. A. Yushkov and V. Yu Kolosov, *J. Alloys Compd.*, 2017, **712**, 418–424.
30 I. Hocaoglu, M. N. Çizmeciyan, R. Erdem, C. Ozen, A. Kurt, A. Sennaroglu and H. Y. Acar, *J. Mater. Chem.*, 2012, **22**, 14674–14681.
31 Q. Ren, Y. Ma, S. Zhang, L. Ga and J. Ai, *ACS Omega*, 2021, **6**, 6361–6367.
32 Q. Liu, Y. Pu, Z. Zhao, J. Wang and D. Wang, *Trans. Tianjin Univ.*, 2020, **26**, 273–282.
33 Y. Xu, J. Suthar, R. Egbu, A. J. Weston, A. M. Fogg and G. R. Williams, *J. Solid State Chem.*, 2018, **258**, 320–327.
34 J. Xue, H. Li, J. Liu, Y. Wang, Y. Liu, D. Sun, W. Wang, L. Huang and J. Tang, *Mater. Lett.*, 2019, **242**, 143–146.
35 L. Dong, Y. Chu, Y. Liu and L. Li, *J. Colloid Interface Sci.*, 2008, **317**, 485–492.
36 W. Yang, T. Xie, T. Jiang and D. Wang, *Colloids Surf., A*, 2013, **433**, 55–58.
37 M. Shakouri-Arani and M. Salavati-Niasari, *Spectrochim. Acta, Part A*, 2014, **133**, 463–471.
38 S. I. Sadovnikov, Y. V. Kuznetsova and A. A. Rempel, *Nano-Struct. Nano-Objects*, 2016, **7**, 81–91.
39 D. O. Vardar, S. Aydin, I. Hocaoglu, F. H. Y. Acar and N. Basaran, *Chem.-Biol. Interact.*, 2018, **291**, 212–219.
40 O. V. Ovchinnikov, I. G. Grevtseva, M. S. Smirnov, T. S. Kondratenko, A. S. Perepelitsa, S. V. Aslanov, V. U. Khokhlov, E. P. Tatyanina and A. S. Matsukovich, *Opt. Quantum Electron.*, 2020, **52**, 198.
41 S. I. Sadovnikov, A. I. Gusev, E. Y. Gerasimov and A. A. Remple, *Inorg. Mater.*, 2016, **52**, 441–446.
42 A. D. Iacovo, C. Venettacci, L. Colace, L. Scopa and S. Foglia, *Sci. Rep.*, 2016, **6**, 37913.
43 M. H. S. A. Hamid, M. A. Ali, A. H. Mirza, P. V. Bernhardt, B. Moubaraki and K. S. Murray, *Inorg. Chim. Acta*, 2009, **362**, 3648–3656.
44 X. Zhang, M. Liu, H. Liu and S. Zhang, *Biosens. Bioelectron.*, 2014, **56**, 307–312.
45 CLSI, *Performance standards for antimicrobial disk susceptibility tests; approved standard, M02-A13*, Clinical and Laboratory Standards Institute, Wayne, PA, USA, 12th edn, 2018.
46 P. R. Murray, E. J. Baron, M. A. Pfaller, F. C. Tenover and R. H. Yolken, *Manual of Clinical Microbiology*, ASM, Washington, DC, 7th edn, 1999.
47 A. M. Clark, A. S. El-Feraly and W. -S. Li, *J. Pharm. Sci.*, 1981, **70**, 951–952.
48 T. S. Rejiniemon, M. V. Arasu, V. Duraipandiyan, K. Ponmurugan, N. A. Al-Dhabi, S. Arokiyaraj, P. Agastian and K. C. Choi, *Ann. Clin. Microbiol. Antimicrob.*, 2014, **13**, 1–9.
49 F. Khan, J. W. Lee, D. T. N. Pham, J. H. Lee, H. W. Kim, Y. K. Kim and Y. M. Kim, *Appl. Microbiol. Biotechnol.*, 2020, **104**, 799–816.
50 M. Imran, M. Imran and S. Khan, *J. Appl. Pharm. Sci.*, 2017, **7**, 168–174.
51 P. Parvekar, J. Palaskar, S. Metgud, R. Maria and S. Dutta, *Biomater. Invest. Dent.*, 2020, **7**, 105–109.
52 R. S. Christy, J. T. T. Kumaran and C. Bansal, *Adv. Sci. Focus*, 2014, **2**, 115–120.
53 J. Sun, W. Yu, A. Usman, T. T. Isimjan, S. DGobbo, E. Alarousu, K. Takanabe and O. F. Mohammed, *J. Phys. Chem. Lett.*, 2014, **5**, 659–665.
54 G. A. Bowmaker, Effendy, P. C. Junk, B. W. Skelton and A. H. White, *Z. Naturforsch., B: Chem. Sci.*, 2004, **59**, 1277–1292.
55 Y.-Y. Kim and D. Walsh, *Nanoscale*, 2010, **2**, 240–247.
56 M. Das and S. E. Livingstone, *Inorg. Chim. Acta*, 1976, **19**, 5–10.
57 M. A. Ali and M. T. H. Tarafdar, *J. Inorg. Nucl. Chem.*, 1977, **39**, 1785–1791.
58 T. S. Kondratenko, A. I. Zvyagin, M. S. Smirnov, I. G. Grevtseva, A. S. Perepelitsa and O. V. Ovchinnikov, *J. Lumin.*, 2019, **208**, 193–200.
59 G. Wang, J. Liu, L. Zhu, Y. Guo and L. Yang, *RSC Adv.*, 2019, **9**, 29936.
60 Y. Zhang, Y. Liu, C. Li, X. Chen and W. Wang, *J. Phys. Chem. C*, 2014, **118**, 4918–4923.
61 S. I. Sadovnikov and A. I. Gusev, *J. Mater. Chem. A*, 2017, **5**, 17676.
62 V. Nandwana, K. E. Elkins, N. Poudyal, G. S. Chaubey, K. Yano and J. P. Liu, *J. Phys. Chem. C*, 2007, **111**, 4185–4189.
63 D. W. Lucey, D. J. MacRae, M. Furis, Y. Sahoo, A. N. Cartwright and P. N. Prasad, *Chem. Mater.*, 2005, **17**, 3754–3762.

64 C. Siva, C. N. Iswarya, P. Baraneedharan and M. Sivakumar, *Mater. Lett.*, 2014, **134**, 56–59.
65 N. Gaponik, D. V. Talapin, A. L. Rogach, H. Kathrin, E. V. Shevchenko, K. Andreas, A. Eychmüller and H. Weller, *J. Phys. Chem. B*, 2002, **106**, 7177–7185.
66 K. Y. Rhee and D. F. Gardiner, *Clin. Infect. Dis.*, 2004, **39**, 755–756.
67 I. A. Mir, V. S. Radhakrishanan, K. Rawat, T. Prasad and H. B. Bohidar, *Sci. Rep.*, 2018, **8**, 9322–9333.
68 K. Rajendiran, Z. Zhao, D. S. Pei and A. Fu, *Polymers*, 2019, **11**, 1–13.
69 H. S. Devi, M. A. Boda, M. A. Shah, S. Parveen and A. H. Wani, *Green Process. Synth.*, 2019, **8**, 38–45.
70 K.-J. Kim, W. S. Sung, S.-K. Moon, J.-S. Chooi, J. G. Kim and D. G. Lee, *J. Microbiol. Biotechnol.*, 2008, **8**, 1482–1484.
71 P. M. S. Sousa, *Rev. Colomb. Cienc. Quim.-Farm.*, 2020, **49**, 374–386.
72 Z. L. Shaw, S. Kuriakose, S. Cheeseman, M. D. Dickey, J. Genzer, A. J. Christofferson, R. J. Crawford, C. F. McConville, J. Chapman, V. K. Truong, A. Elbourne and S. Walia, *Nat. Commun.*, 2021, **12**, 3897.
73 R. Javed, M. Zia, S. Naz, S. O. Aisida, N. Ain and Q. Ao, *J. Nanobiotechnol.*, 2020, **18**, 172.
74 D. A. Geraldo, N. Arancibia-Miranda, N. A. Villagra, G. C. Mora and R. Arratia-Perez, *J. Nanopart. Res.*, 2012, **14**, 1286–1294.
75 K. Zheng, M. I. Setyawati, D. T. Leong and J. Xie, *ACS Nano*, 2017, **11**, 6904–6910.
76 Z. Li, L. Wu, H. Wang, W. Zhou, H. Liu, H. Cui, P. Li, P. K. Chu and X.-F. Yu, *ACS Appl. Nano Mater.*, 2019, **2**, 1202–1209.
77 P. Patra, S. Roy, S. Sarkar, S. Mitra, S. Pradhan, N. Debnath and A. N. Goswami, *Appl. Nanosci.*, 2015, **5**, 857–866.
78 A. Dasari and V. Guttena, *J. Photochem. Photobiol., B*, 2016, **157**, 57–69.
79 S. Ostrovsky, G. Kazimirsky, A. Gedanken and C. Brodie, *Nano Res.*, 2009, **2**, 882–890.
80 E. Kamyab, S. Rohde, M. Y. Kellermann and P. J. Schupp, *Molecules*, 2020, **25**, 4808.